

Higgs Boson Production at Hadron Colliders

with Soft Gluon Effects: I. Backgrounds

C. Balázs^{1,2*} and C.-P. Yuan^{1†}

¹ *Michigan State University, East Lansing, MI 48824, U.S.A.*

² *Fermi National Accelerator Laboratory, Batavia, Illinois 60510, USA*

hep-ph/9810319

FERMILAB-PUB-98/202-T

CTEQ-815

MSUHEP-80519

Abstract

The gold-plated discovery mode of a Standard Model like Higgs boson at the CERN Large Hadron Collider (LHC) is the $H \rightarrow Z^0 Z^0$ decay mode. To find and then measure the properties of the Higgs, it is crucial to have the most precise theoretical prediction both for the signal and the QCD background in this mode. In this work we calculate the effects of the initial-state multiple soft-gluon emission on the kinematic distributions of Z^0 boson and photon pairs produced in hadron collisions. The Collins-Soper-Sterman formalism is extended to resum the large logarithmic terms due to soft-gluons. The resummed total rates, the invariant mass, transverse momentum, and rapidity distributions of the Z^0 and photon pairs, and the transverse momentum distributions of the individual vector bosons are presented and compared to the fixed order predictions in the whole kinematic range, for the LHC energies and for the upgraded Fermilab Tevatron. Our conclusion is that the resummed predictions should be used when extracting the Higgs signal at the LHC.

PACS numbers: 12.38.-t, 12.38.Cy, 13.85.Qk.

Typeset using REVTeX

*E-mail address: balazs@pa.msu.edu

†E-mail address: yuan@pa.msu.edu

I. INTRODUCTION

The underlying dynamics of the electroweak symmetry breaking sector of the Standard Model (SM) awaits understanding. The principal goal of the CERN Large Hadron Collider (LHC) is to shed light on this open question. The direct searches at the CERN Large Electron Positron (LEP) collider have constrained the mass of the SM Higgs boson to be higher than 90 GeV [1]. Furthermore, global analyses of electroweak data [2] and the values of the top quark and the W^\pm boson masses [3] suggest that the SM Higgs boson is light, less than a few hundred GeV. Arguments based on supersymmetry (SUSY) also indicate that the lightest Higgs boson is lighter than the top quark [4]. Hence, the existence of a light Higgs boson is highly possible.

It has been shown in the literature that a SM like Higgs boson with a mass less than or about 120 GeV can be detected at the upgraded Fermilab Tevatron via $p\bar{p} \rightarrow W^\pm (\rightarrow \ell^\pm \nu) H (\rightarrow b\bar{b}, \tau^+\tau^-)$ [5], or $p\bar{p}(gg) \rightarrow H (\rightarrow W^*W^* \rightarrow \ell\nu jj$ and $\ell\nu\ell\nu)$ [6], and a SUSY Higgs boson can be detected in the $W^\pm h$ and $hb\bar{b}$ modes [7]. To observe a light ($m_H < 120$ GeV) neutral Higgs boson at the LHC, the most promising detection mode is the di-photon channel $H \rightarrow \gamma\gamma$ [8] via the production process $pp(gg) \rightarrow HX$. In the intermediate mass ($120 \text{ GeV} < m_H < 2 m_Z$) region, the $Z^{0*}Z^0$ channel is also useful in addition to the $\gamma\gamma$ channel [8]. If the Higgs boson is heavier than twice the mass of the Z^0 boson, the gold-plated decay mode into two Z^0 bosons (which sequentially decay into leptons) [8] is the best way to detect it. At the LHC, as at any hadron–hadron collider, initial–state radiative corrections from Quantum Chromodynamics (QCD) interaction to electroweak processes can be large. Some fixed order QCD corrections have been calculated to the Higgs signal and to its most important backgrounds [9–12]. The next-to-leading order (NLO) corrections to the total cross section of $pp(gg) \rightarrow HX$ have been found to be large (50-100 %) [9], and the largest contribution in the fixed order corrections results from soft gluon emission [13]. This signals the slow convergence of the perturbative series, and the importance of still higher order corrections. Furthermore, the fixed order corrections fail to predict the

transverse momentum distributions of the Higgs boson and its decay products correctly. The knowledge of these distributions is necessary to precisely predict the signal and the background in the presence of various kinematic cuts, in order to deduce the accurate event rates to compare with theory predictions [14]. To predict the correct distribution of the transverse momentum of the photon or Z^0 pair and the individual vector bosons, or the kinematical correlation of the two vector bosons produced at hadron colliders, it is necessary to include the effects from the initial-state multiple soft-gluon emission. In this work, we present the results of our calculation for the most important continuum backgrounds to the Higgs boson signal detected at hadron colliders. The distributions of the Higgs boson signal for the $h_1 h_2 \rightarrow H \rightarrow \gamma\gamma X$ and $Z^0 Z^0 X$ processes, including the soft-gluon effects, will be discussed in our future work [15].

In scattering processes involving hadrons, the dynamics of the multiple soft-gluon radiation can be described by the resummation technique. We extend the Collins–Soper–Sterman (CSS) resummation formalism [16–18] to describe the production of photon and Z^0 pairs. This extension is analogous to our recent resummed calculation of the hadronic production of photon pairs [19]. In comparison, an earlier work [20] on the soft-gluon resummation for the $q\bar{q} \rightarrow Z^0 Z^0 X$ process did not include the complete NLO corrections. In the present work, the effect of initial-state multiple soft-gluon emission in $q\bar{q} \rightarrow Z^0 Z^0 X$ is resummed with the inclusion of the full NLO contributions, so that the inclusive rate of the Z^0 boson pair production agrees with the NLO result presented in Ref. [10]. Furthermore, we also include part of the higher order contributions in our results by using the CSS resummation formalism.

The collected di-photon data at the Tevatron, a $p\bar{p}$ collider with center-of-mass energy $\sqrt{S} = 1.8$ TeV with 84 and 81 pb^{-1} integrated luminosity (for CDF and DØ), are in the order of 10^3 events per experiment [21,22]. After the upgrade of the Tevatron, with $\sqrt{S} = 2$ TeV and a 2 fb^{-1} integrated luminosity, about 4×10^4 photon pairs can be detected, and more than 3×10^3 Z^0 boson pairs can be produced. At the LHC, a $\sqrt{S} = 14$ TeV pp collider with a 100 fb^{-1} integrated luminosity, we expect about 6×10^6 photon and 1.5×10^6 Z^0

pairs to be produced, after imposing the kinematic cuts described later in the text. This large data sample will play an important role in the search for the Higgs boson(s) and new physics that modifies the production of the vector boson pairs (e.g., by altering the vector boson tri-linear couplings [23]).

The rest of this paper is organized as follows. Section II briefly summarizes the extension of the CSS resummation formalism to the Z^0Z^0 pair production. In Section III, the numerical results of the resummed and fixed order calculations are compared for various distributions of the photon and Z^0 pairs produced at the LHC and the upgraded Tevatron. Section IV contains our conclusions.

II. ANALYTICAL RESULTS

A. The CSS Resummation Formalism for Z^0 Pair Production

When QCD corrections to the Z^0 boson pair production cross section are calculated order by order in the strong coupling constant α_s , the emission of potentially soft gluons spoils the convergence of the perturbative series for small transverse momenta (Q_T) of the Z^0 boson pair. In the $Q_T \ll Q$ region, the cross section can be written as [18]

$$\lim_{Q_T \rightarrow 0} \frac{d\sigma}{dQ_T^2} = \sum_{n=1}^{\infty} \sum_{m=0}^{2n-1} \alpha_s^n \frac{{}_n v_m}{Q_T^2} \ln^m \left(\frac{Q^2}{Q_T^2} \right) + \mathcal{O} \left(\frac{1}{Q_T} \right),$$

where Q is the invariant mass of the Z^0 boson pair, and the coefficients ${}_n v_m$ are perturbatively calculable. At each order of the strong coupling the emitted gluon(s) can be soft and/or collinear, which yields a small Q_T . When the two scales Q and Q_T are very different, the logarithmic terms $\ln^m(Q^2/Q_T^2)$ are large, and for $Q_T \ll Q$ the perturbative series is dominated by these terms. It was shown in Refs. [16–18] that these logarithmic contributions can be summed up to all order in α_s , resulting in a well behaved cross section in the full Q_T region.

The resummed differential cross section of the Z^0 boson pair production in hadron collisions is written, similarly to the cross sections of the lepton pair production [24], or photon

pair production [19], in the form:

$$\begin{aligned}
\frac{d\sigma(h_1 h_2 \rightarrow Z^0 Z^0 X)}{dQ^2 dy dQ_T^2 d\cos\theta d\phi} &= \frac{1}{48\pi S} \frac{\beta}{Q^2} \\
&\times \left\{ \frac{1}{(2\pi)^2} \int d^2 b e^{i\vec{Q}_T \cdot \vec{b}} \sum_{i,j} \widetilde{W}_{ij}(b_*, Q, x_1, x_2, \theta, \phi, C_{1,2,3}) \widetilde{W}_{ij}^{NP}(b, Q, x_1, x_2) \right. \\
&\left. + Y(Q_T, Q, x_1, x_2, \theta, \phi, C_4) \right\}. \tag{1}
\end{aligned}$$

In this case, the variables Q , y , and Q_T are the invariant mass, rapidity, and transverse momentum of the Z^0 boson pair in the laboratory frame, while θ and ϕ are the polar and azimuthal angle of one of the Z^0 bosons in the Collins-Soper frame [25]. The factor

$$\beta = \sqrt{1 - \frac{4m_Z^2}{Q^2}}$$

originates from the phase space for producing the massive Z^0 boson pair. The parton momentum fractions are defined as $x_1 = e^y Q / \sqrt{S}$, and $x_2 = e^{-y} Q / \sqrt{S}$, and \sqrt{S} is the center-of-mass (CM) energy of the hadrons h_1 and h_2 .

The renormalization group invariant function $\widetilde{W}_{ij}(b)$ sums the large logarithmic terms $\alpha_s^n \ln^m(b^2 Q^2)$ to all orders in α_s . For a scattering process initiated by the partons i and j ,

$$\begin{aligned}
\widetilde{W}_{ij}(b, Q, x_1, x_2, \theta, \phi, C_{1,2,3}) &= \exp \{-\mathcal{S}_{ij}(b, Q, C_{1,2})\} \\
&\times \left[\mathcal{C}_{i/h_1}(x_1, b, C_{1,2,3}, t, u) \mathcal{C}_{j/h_2}(x_2, b, C_{1,2,3}, t, u) \right. \\
&\left. + \mathcal{C}_{j/h_1}(x_1, b, C_{1,2,3}, u, t) \mathcal{C}_{i/h_2}(x_2, b, C_{1,2,3}, u, t) \right] \\
&\times \mathcal{F}_{ij}(\alpha(C_2 Q), \alpha_s(C_2 Q), \theta, \phi). \tag{2}
\end{aligned}$$

Here the Sudakov exponent $\mathcal{S}_{ij}(b, Q, C_{1,2})$ is defined as

$$\mathcal{S}_{ij}(b, Q, C_{1,2}) = \int_{C_1^2/b^2}^{C_2^2 Q^2} \frac{d\bar{\mu}^2}{\bar{\mu}^2} \left[A_{ij}(\alpha_s(\bar{\mu}), C_1) \ln \left(\frac{C_2^2 Q^2}{\bar{\mu}^2} \right) + B_{ij}(\alpha_s(\bar{\mu}), C_1, C_2) \right]. \tag{3}$$

In Eq. (2), \mathcal{F}_{ij} originates from the hard scattering process, and will be given later for specific initial state partons. $\mathcal{C}_{i/h}(x)$ denotes the convolution of the perturbative Wilson coefficient functions C_{ia} with parton distribution functions (PDF) $f_{a/h}(\xi)$ (describing the probability density of parton a inside hadron h with momentum fraction ξ):

$$\begin{aligned} \mathcal{C}_{i/h}(x, b, C_{1,2,3}, t, u) = \\ \sum_a \int_x^1 \frac{d\xi}{\xi} C_{ia} \left(\frac{x}{\xi}, b, \mu = \frac{C_3}{b}, C_1, C_2, t, u \right) f_{a/h} \left(\xi, \mu = \frac{C_3}{b} \right). \end{aligned} \quad (4)$$

The invariants s , t and u are defined for the $q(p_1)\bar{q}(p_2) \rightarrow Z^0(p_3)Z^0(p_4)$ subprocess as

$$s = (p_1 + p_2)^2, \quad t = (p_1 - p_3)^2, \quad u = (p_2 - p_3)^2, \quad (5)$$

with $s + t + u = 2m_Z^2$.

The functions A_{ij} , B_{ij} and C_{ij} are calculated perturbatively in powers of α_s/π :

$$\begin{aligned} A_{ij}(\alpha_s(\bar{\mu}), C_1) &= \sum_{n=1}^{\infty} \left(\frac{\alpha_s(\bar{\mu})}{\pi} \right)^n A_{ij}^{(n)}(C_1), \\ B_{ij}(\alpha_s(\bar{\mu}), C_1, C_2) &= \sum_{n=1}^{\infty} \left(\frac{\alpha_s(\bar{\mu})}{\pi} \right)^n B_{ij}^{(n)}(C_1, C_2), \\ C_{ij}(z, b, \mu, C_1, C_2, t, u) &= \sum_{n=0}^{\infty} \left(\frac{\alpha_s(\mu)}{\pi} \right)^n C_{ij}^{(n)}(z, b, C_1, C_2, t, u). \end{aligned}$$

The dimensionless constants C_1 , C_2 and $C_3 \equiv \mu b$ were introduced in the solution of the renormalization group equations for \widetilde{W}_{ij} . Their canonical choice is $C_1 = C_3 = 2e^{-\gamma_E} \equiv b_0$, $C_2 = C_1/b_0 = 1$, and $C_4 = C_2 = 1$ [18], where γ_E is the Euler constant.

For large b , which is relevant for small Q_T , the perturbative evaluation of Eq. (2) is questionable. Thus in Eq. (1), \widetilde{W}_{ij} is evaluated at $b_* = b/\sqrt{1 + (b/b_{\max})^2}$, so that the perturbative calculation is reliable. Here b_{\max} is a free parameter of the formalism [18] that has to be constrained by other data (e.g. Drell–Yan), along with the non-perturbative function $\widetilde{W}_{ij}^{NP}(b)$ which is introduced in Eq. (1) to parametrize the incalculable long distance effects. Since the $q\bar{q} \rightarrow \gamma\gamma$ or Z^0Z^0 , and the $q\bar{q} \rightarrow V \rightarrow \ell\ell'$ processes have the same initial state as well as the same QCD color structure, in this work we assume that the non-perturbative function $\widetilde{W}_{ij}^{NP}(b)$, fitted to existing low energy Drell-Yan data [26], also describes the non-perturbative effects in the $q\bar{q} \rightarrow \gamma\gamma$ and Z^0Z^0 processes. Needless to say, this assumption has to be tested by experimental data.

The function Y in Eq. (1) contains contributions from the NLO calculation that are less singular than $1/Q_T^2$ or $\ln(Q^2/Q_T^2)/Q_T^2$ as $Q_T \rightarrow 0$. This function restores the regular contribution in the fixed order perturbative calculation that is not included in the resummed

piece \widetilde{W}_{ij} . In the Y function, both the factorization and the renormalization scales are chosen to be $C_4 Q$. The detailed description of the matching (or “switching”) between the resummed and the fixed order cross sections for $Q_T \sim Q$ can be found in Ref. [24].

B. The $q\bar{q}$, qg and $\bar{q}g \rightarrow Z^0 Z^0 X$ subprocesses

The largest background to the Higgs boson signal in the $Z^0 Z^0$ channel is the continuum production of Z^0 boson pairs via the $q\bar{q} \rightarrow Z^0 Z^0 X$ partonic subprocess [27]. The next-to-leading order calculations of this process are given in Refs. [10,11]. A representative set of Feynman diagrams, included in the NLO calculations, is shown in Fig. 1. The application of the CSS resummation formalism for the $q\bar{q} \rightarrow Z^0 Z^0 X$ subprocess is the same as that for the case of $q\bar{q} \rightarrow \gamma\gamma X$ [19]. The $A^{(1)}$, $A^{(2)}$ and $B^{(1)}$ coefficients in the Sudakov exponent are identical to those of the Drell–Yan case. This follows from the observation that to produce a heavy Z^0 boson pair, the virtual–quark line connecting the two Z^0 bosons in Fig. 1 is far off the mass shell, and the leading logarithms due to soft gluon emission beyond the leading order can only be generated from the diagrams in which soft gluons are connected to the incoming (anti–)quark. This situation was described in more detail for di-photon production [19].

The resummed cross section is given by Eq. (1), with i and j representing quark and anti–quark flavors, respectively, and

$$\mathcal{F}_{ij}(g, g_s, \theta, \phi) = 2\delta_{ij}(g_L^2 + g_R^2)^2 \frac{1 + \cos^2 \theta}{1 - \cos^2 \theta}.$$

The left- and right-handed couplings $g_{L,R}$ are defined through the $q\bar{q}Z^0$ vertex, which is written as $i\gamma_\mu [g_L(1 - \gamma_5) + g_R(1 + \gamma_5)]$, with

$$g_L = g \frac{T_3 - s_w^2 Q_f}{2c_w} \quad \text{and} \quad g_R = -g \frac{s_w^2 Q_f}{2c_w}. \quad (6)$$

Here g is the weak coupling constant, T_3 is the third component of the $SU(2)_L$ generator ($T_3 = 1/2$ for the up quark Q_u , and $-1/2$ for the down quark Q_d), s_w (c_w) is the sine (cosine)

of the weak mixing angle, and Q_f is the electric charge of the incoming quark in the units of the positron charge ($Q_u = 2/3$ and $Q_d = -1/3$). The values of these parameters will be given in the next section.

The explicit forms of the A and B functions, used in the numerical calculations are:

$$\begin{aligned} A_{q\bar{q}}^{(1)}(C_1) &= C_F, \\ A_{q\bar{q}}^{(2)}(C_1) &= C_F \left[\left(\frac{67}{36} - \frac{\pi^2}{12} \right) N_C - \frac{5}{18} N_f - 2\beta_1 \ln \left(\frac{b_0}{C_1} \right) \right], \\ B_{q\bar{q}}^{(1)}(C_1, C_2) &= C_F \left[-\frac{3}{2} - 2 \ln \left(\frac{C_2 b_0}{C_1} \right) \right], \end{aligned} \quad (7)$$

where N_f is the number of light quark flavors, $N_C = 3$ is the number of colors in QCD, $C_F = 4/3$, and $\beta_1 = (11N_C - 2N_f)/12$.

To obtain the value of the total cross section to NLO, it is necessary to include the Wilson coefficients $C_{ij}^{(0)}$ and $C_{ij}^{(1)}$, which can be derived similarly to those for di-photon production [19]. The results are:

$$\begin{aligned} C_{jk}^{(0)}(z, b, \mu, \frac{C_1}{C_2}, t, u) &= \delta_{jk} \delta(1-z), \\ C_{jG}^{(0)}(z, b, \mu, \frac{C_1}{C_2}, t, u) &= 0, \\ C_{jk}^{(1)}(z, b, \mu, \frac{C_1}{C_2}, t, u) &= \delta_{jk} C_F \left\{ \frac{1}{2}(1-z) - \frac{1}{C_F} \ln \left(\frac{\mu b}{b_0} \right) P_{j \leftarrow k}^{(1)}(z) \right. \\ &\quad \left. + \delta(1-z) \left[-\ln^2 \left(\frac{C_1}{b_0 C_2} e^{-3/4} \right) + \frac{\mathcal{V}(t, u)}{4} + \frac{9}{16} \right] \right\}, \\ C_{jG}^{(1)}(z, b, \mu, \frac{C_1}{C_2}, t, u) &= \frac{1}{2} z(1-z) - \ln \left(\frac{\mu b}{b_0} \right) P_{j \leftarrow G}^{(1)}(z). \end{aligned} \quad (8)$$

In the above expressions, the splitting kernels are [28]

$$\begin{aligned} P_{j \leftarrow k}^{(1)}(z) &= C_F \left(\frac{1+z^2}{1-z} \right)_+ \quad \text{and} \\ P_{j \leftarrow G}^{(1)}(z) &= \frac{1}{2} [z^2 + (1-z)^2]. \end{aligned} \quad (9)$$

For Z^0 boson pair production the function \mathcal{V} in Eq. (7) is given by

$$\mathcal{V}(t, u) = \mathcal{V}_{Z^0 Z^0}(t, u) = -4 + \frac{\pi^2}{3} + \frac{tu}{t^2 + u^2} (F(t, u) + F(u, t) - 2).$$

The definition of the function $F(t, u)$ is somewhat lengthy and can be found in Appendix C of Ref. [10] (cf. Eqs. (C1) and (C2)). The function $\mathcal{V}(t, u)$ depends on the kinematic correlation between the initial and final states through its dependence on t and u . In the $m_Z \rightarrow 0$ limit, $F(t, u) + F(u, t)$ reduces to $F^{virt}(t, u)$ of the di-photon case which is given in Ref. [19].¹

The non-perturbative function used in this study is [26]

$$\widetilde{W}_{q\bar{q}}^{NP}(b, Q, Q_0, x_1, x_2) = \exp \left[-g_1 b^2 - g_2 b^2 \ln \left(\frac{Q}{2Q_0} \right) - g_1 g_3 b \ln (100x_1 x_2) \right],$$

with $g_1 = 0.11 \text{ GeV}^2$, $g_2 = 0.58 \text{ GeV}^2$, $g_3 = -1.5 \text{ GeV}^{-1}$, and $Q_0 = 1.6 \text{ GeV}$. These values were fit for the CTEQ2M parton distribution function, with the canonical choice of the renormalization constants, i.e. $C_1 = C_3 = b_0$ and $C_2 = 1$, and $b_{max} = 0.5 \text{ GeV}^{-1}$ was used. In principle, these coefficients should be refit for CTEQ4M distributions [30] used in this study. We have checked that using the updated fit in Ref. [31] does not change largely our conclusion because at the LHC and Tevatron energies the perturbative Sudakov contribution is more important compared to that in the low energy fixed target experiments.

Before concluding this section we note that for the di-photon production, we use the formalism described in Ref. [19] to include the $gg \rightarrow \gamma\gamma X$ contribution, in which part of the higher order corrections has been included via resummation. Since a gauge invariant calculation of the $gg \rightarrow Z^0 Z^0 g$ cross section in the SM involves diagrams with the Higgs particle, we shall defer its discussion to a separate work [15].

¹This is connected to the fact that as $m_Z \rightarrow 0$ the virtual corrections of the Z^0 pair and di-photon productions are the same (up to the couplings), which is apparent when comparing Eq.(11) of Ref. [29] and Eq.(12) of Ref. [10], after including a missing factor of $1/(16\pi s)$ in the latter equation.

III. NUMERICAL RESULTS

We implemented our analytic results in the ResBos Monte Carlo event generator [24]. As an input we use the following electroweak parameters [32]:

$$G_F = 1.16639 \times 10^{-5} \text{ GeV}^{-2}, \quad m_Z = 91.187 \text{ GeV}, \quad m_W = 80.41 \text{ GeV}, \quad \alpha(m_Z) = \frac{1}{128.88}.$$

In the on-shell renormalization scheme we define the effective weak mixing angle

$$\sin^2 \theta_w^{eff} = 1 - \frac{m_W^2}{\rho m_Z^2},$$

with

$$\rho = \frac{m_W^2}{m_Z^2} \left(1 - \frac{\pi \alpha(m_Z)}{\sqrt{2} G_F m_W^2} \right)^{-1}.$$

In Eq.(6), the coupling of the Z^0 boson to fermions, g , is defined using the improved Born approximation:

$$g^2 = 4\sqrt{2}G_F(c_w^{eff})^2 m_Z^2 \rho,$$

with $c_w^{eff} = \sqrt{1 - \sin^2 \theta_w^{eff}}$, the cosine of the effective weak mixing angle. (In Eq. (6) c_w is identified with c_w^{eff} .) We use the NLO expression for the running strong and electroweak couplings $\alpha_s(\mu)$ and $\alpha(\mu)$, as well as the NLO parton distribution function CTEQ4M (defined in the modified minimal subtraction, i.e. $\overline{\text{MS}}$, scheme), unless stated otherwise. Furthermore, in all cases we set the renormalization scale equal to the factorization scale: $\mu_R = \mu_F = Q$.

Table I summarizes the total rates for the leading order (LO), i.e. $\mathcal{O}(\alpha_s^0)$, and resummed photon- and Z^0 -pair production cross sections for the LHC and the Tevatron. For the lowest order calculation we show results using LO (CTEQ4L) and NLO (CTEQ4M) parton distributions, because there is a noticeable difference due to the PDF choice. As it was discussed in Ref. [24], the resummed total rate is expected to reproduce the $\mathcal{O}(\alpha_s)$ rate, provided that in the resummed calculation the $A^{(1)}$, $B^{(1)}$ and $C^{(1)}$ coefficients and the $\mathcal{O}(\alpha_s)$ Y piece are included, and the Q_T distribution is described by the resummed result for $Q_T \leq Q$ and by the $\mathcal{O}(\alpha_s)$ result for $Q_T > Q$. In our present calculation we added the $A^{(2)}$

coefficient to include the most important higher order corrections in the Sudakov exponent. Our matching prescription (cf. Ref. [24]) is to switch from the resummed prediction to the fixed-order perturbative calculation as they cross around $Q_T \sim Q$. This switch is performed for any given Q and y of the photon or Z^0 boson pairs. In the end, the total cross section predicted by our resummed calculation is about the same as that predicted by the NLO calculation. The small difference of those two predictions can be interpreted as an estimate of the contribution beyond the NLO.

A. Z^0 pair production at the LHC

In the LHC experiments the $H \rightarrow Z^0 Z^0$ channel can be identified through the decay products of the Z^0 bosons. The detailed experimental kinematic cuts for this process are given in Ref. [8]. Since the aim of this work is not to analyze the decay kinematics of the background, rather to present the effects of the initial-state soft-gluon radiation, following Ref. [10] for the LHC energies we restrict the rapidities of each Z^0 bosons as: $|y^Z| < 3.0$. We do not apply any other kinematic cuts. The total rates are given in Table I. Our $\mathcal{O}(\alpha_s^0)$ rates are in agreement with that of Ref. [10] when calculated using the same PDF. We expect the resummed rate to be higher than the $\mathcal{O}(\alpha_s)$ rate due to the inclusion of the $A^{(2)}$ term. Indeed, our K factor, defined as the ratio of the resummed to the LO rate using the same PDF in both calculations, is higher than the naive soft gluon K -factor ($K_{\text{naive}} = 1 + 8\pi\alpha_s(Q)/9 \sim 1.3$) of Ref. [33], which estimates the NLO corrections to the production rate of $q\bar{q} \rightarrow Z^0 Z^0 X$ in the DIS (deep-inelastic scattering) scheme. Our K -factor approaches the naive one with the increase of the center-of-mass energy, as expected.

The rates for the different subprocesses of the Z^0 boson pair production are given in Table II. At the LHC the $qg \rightarrow Z^0 Z^0 X$ subprocess contributes about 25% of the $qq + qg \rightarrow Z^0 Z^0 X$ rate. The K -factor is defined as the ratio $\sigma(q\bar{q} + qg \rightarrow Z^0 Z^0 X)/\sigma(q\bar{q} \rightarrow Z^0 Z^0)$, which is about 1.4 for using CTEQ4M PDF.

Figs. 2–4 show our results for proton-proton collisions at the LHC energy, $\sqrt{S} = 14$ GeV.

Fig. 2 shows the transverse momentum distribution of Z^0 pairs. The NLO ($\mathcal{O}(\alpha_s)$) prediction for the $q\bar{q} + qg \rightarrow Z^0 Z^0 X$ subprocesses, shown by the dotted curve, is singular as $Q_T \rightarrow 0$. This singular behavior originates from the contribution of terms which grow at least as fast as $1/Q_T^2$ or $\ln(Q^2/Q_T^2)/Q_T^2$. This, so-called asymptotic part, is shown by the dash-dotted curve, which coincides with the $\mathcal{O}(\alpha_s)$ distribution as $Q_T \rightarrow 0$. After exponentiating these terms, the distribution is well behaved in the low Q_T region, as shown by the solid curve. The resummed curve matches the $\mathcal{O}(\alpha_s)$ curve at about $Q_T = 320$ GeV. Following our matching prescription described in the previous section, we find that this matching takes place around $Q_T = 300$ GeV, depending on the actual values of Q and y . Fig. 2 also shows that at the LHC there is a substantial contribution from qg scattering, which is evident from the difference between the solid and dashed curves, where the dashed curve is the resummed contribution from the $q\bar{q} \rightarrow Z^0 Z^0 X$ subprocesses.

In Fig. 3 we give the integrated distributions, defined as

$$\frac{d\sigma}{dQ_T^{\min}} = \int_{Q_T^{\min}}^{Q_T^{\max}} dQ_T \frac{d\sigma}{dQ_T}, \quad (10)$$

where Q_T^{\max} is the largest Q_T allowed by the phase space. In the NLO calculation, this distribution grows without bound near $Q_T^{\min} = 0$, as a result of the singular behavior of the scattering amplitude when $Q_T \rightarrow 0$. It is clearly shown by Fig. 3 that the Q_T distribution of the resummed calculation is different from that of the NLO calculation. The different shapes of the two curves in Fig. 3 indicates that the predicted Z^0 pair production rates, with a minimal value of the transverse momentum Q_T , are different in the two calculations. This is important at the determination of the background for the detection of a Higgs boson even with moderately large transverse momentum. For $Q_T^{\min} = 50$ GeV, the resummed cross section is about 1.5 times of the NLO cross section.

The invariant mass and the rapidity distributions of the Z^0 boson pairs, and the transverse momentum distribution of the individual Z^0 bosons are shown in Fig 4. When calculating the production rate as the function of the Z^0 pair invariant mass, we integrate the Q_T distribution for any Q , and y . When plotting the transverse momentum distributions of

the individual Z^0 bosons, we include both of the Z^0 bosons per event. In the shape of the invariant mass and rapidity distributions we do not expect large deviations from the NLO results. Indeed, the shape of our invariant mass distribution agrees with that in Ref. [10]. However, the resummed transverse momentum distribution P_T^Z of the individual Z^0 bosons is slightly broader than the NLO distribution (not shown in Fig 4, cf. Ref. [10]). This is expected because, in contrast with the NLO distribution, the resummed transverse momentum distribution of the Z^0 boson pair is finite as $Q_T \rightarrow 0$ so that the P_T^Z distribution is less peaked.

In Figs. 5 and 6 we show the dependence of the resummed result on the values of the renormalization constants C_i ($i = 1, 2$), and the values of the non-perturbative parameters g_i ($i = 1, 2, 3$), respectively. As Eq. (2) shows, both the Sudakov exponent \mathcal{S}_{ij} and the Wilson coefficients $\mathcal{C}_{i/h}$ depend on the renormalization constants C_1 and C_2 . The scale C_1/b determines the onset of the non-perturbative physics, and $C_2 Q$ specifies the scale of the hard scattering process. We vary both C_1 and C_2 by a factor of 2. In Fig. 5, we show that the resummed calculation using the canonical C_1 and C_2 values (upper solid curve) hardly differs from the one which uses $C_1 = b_0/2$ and $C_2 = 1/2$ (lower solid curve). This difference is certainly smaller than the difference between the resummed and fixed order (dashed) curves in the $Q_T^{ZZ} = 50 - 100$ GeV region. In Fig. 6, we show two resummed curves, one with the non-perturbative parameters given at the end of Section II.B (solid curve), and one with the following non-perturbative parameters: $g_1 = 0.15$ GeV 2 , $g_2 = 0.48$ GeV 2 , $g_3 = -0.58$ GeV $^{-1}$, and $Q_0 = 1.6$ GeV (dashed curve, c.f. Ref [31]). There is some difference only in the lowest Q_T^{ZZ} region ($Q_T^{ZZ} < 30$ GeV), and this difference is negligible compared to the difference between the resummed and NLO (dotted) calculations. Based on these results, we conclude that the CSS resummation gives a stable prediction for the gauge boson pair production at the LHC energy, and the same conclusions also hold for the Tevatron.

B. Z^0 Pair Production at the upgraded Tevatron

After the upgrade of the Fermilab Tevatron, there are more than 3×10^3 Z^0 boson pairs to be produced. Since this data sample can be used to test the tri-linear gauge boson couplings [23], we also give our results for the upgraded Tevatron with proton–anti-proton collisions at a center-of-mass energy of 2 TeV. Our kinematic cuts constrain the rapidity of both of the Z^0 bosons such that $|y^Z| < 3$. Both the LO and resummed total rates are listed in Table I. The ratio $\sigma(q\bar{q} + qg \rightarrow Z^0 Z^0 X)/\sigma(q\bar{q} \rightarrow Z^0 Z^0)$ is about 1.6, which is larger than the naive soft gluon K -factor of 1.3. Table II shows that $qg \rightarrow Z^0 Z^0 X$ partonic subprocess contributes only a small amount (about 3%) at this energy, in contrast to 25% at the LHC.

Figs. 7–9 show the resummed predictions for the upgraded Tevatron. The invariant mass and rapidity distributions of Z^0 boson pairs, and the transverse momentum distribution of the individual Z^0 bosons are shown in Fig. 7. The solid curve shows the resummed contributions from the $q\bar{q} + qg \rightarrow Z^0 Z^0 X$ subprocess. The resummed contribution from the $q\bar{q} \rightarrow Z^0 Z^0 X$ subprocess is shown by the dashed curve. The leading order $q\bar{q} \rightarrow Z^0 Z^0$ cross section is also shown, by the dash-dotted curve. The invariant mass distribution of the $q\bar{q} + qg \rightarrow Z^0 Z^0 X$ subprocess is in agreement with the NLO result of Ref. [10], when calculated for $\sqrt{S} = 1.8$ TeV. From this figure we also find that the contribution from the $qg \rightarrow Z^0 Z^0 X$ subprocess at the energy of the Tevatron is very small.

In Fig. 8 we compare the NLO and resummed distributions of the transverse momentum of the Z^0 pair. The figure is qualitatively similar to that at the LHC, as shown in Fig. 2. The resummed and the NLO curves merge at about 100 GeV. The resummed contribution from the $q\bar{q} \rightarrow Z^0 Z^0 X$ subprocess is shown by the dashed curve, which clearly dominates the total rate.

In Fig. 9 we show the integrated distribution $d\sigma/dQ_T^{\min}$ for Z^0 boson pair production at the upgraded Tevatron. The figure is qualitatively the same as that for the LHC (cf. Fig. 3). The NLO curve runs well under the resummed one in the $Q_T^{\min} < 80$ GeV region, and the Q_T distributions from the NLO and the resummed calculations have different shapes even

in the region where Q_T is of the order 60 GeV. For $Q_T^{min} = 30$ GeV, the resummed rate is about 1.5 times of the NLO rate.

C. Di-photon production at the LHC

Photon pairs from the decay process $H \rightarrow \gamma\gamma$ can be directly detected at the LHC. When calculating its most important background rates, we impose the kinematic cuts on the final state photons that reflect the optimal detection capabilities of the ATLAS detector [8]:

$p_T^\gamma > 25$ GeV, for the transverse momentum of each photons,

$|y^\gamma| < 2.5$, for the rapidity of each photons, and

$p_T^1/(p_T^1+p_T^2) < 0.7$, to suppress the fragmentation contribution, where p_T^1 is the transverse momentum of the photon with the higher p_T value.

We also apply a $\Delta R = 0.4$ separation cut on the photons, but our results are not sensitive to this cut. (This conclusion is similar to that in Ref. [19].) The total rates and cross sections from the different partonic subprocesses are presented in Tables I and III. We have incorporated part of the higher order contributions to this process by including $A^{(2)}$ in the Sudakov factor and $C_{gg}^{(1)}$ in the Wilson coefficient functions (cf. Ref. [19]). Within this ansatz, up to $\mathcal{O}(\alpha_s^3)$, the $gg \rightarrow \gamma\gamma X$ rate is about 24 pb, which increases the total K -factor by almost 1.0. The leading order $gg \rightarrow \gamma\gamma$ rate, via the box diagram, is about 22 pb and 14 pb for using the LO PDF CTEQ4L and the NLO PDF CTEQ4M, respectively. The large difference mainly due to the differences in the strong coupling constants used in the two calculations²: CTEQ4L requires $\alpha_s(m_Z) = 0.132$, while for CTEQ4M $\alpha_s(m_Z) = 0.116$. The ratio $\sigma(q\bar{q} + qg \rightarrow \gamma\gamma X)/\sigma(q\bar{q} \rightarrow \gamma\gamma)$ is 1.5, and $\sigma(gg \rightarrow \gamma\gamma X)/\sigma(q\bar{q} \rightarrow \gamma\gamma)$ is about 1. Hence, the ratio of the resummed and the $\mathcal{O}(\alpha_s^0)$ rates, is quite substantial.

Figs. 10–12 show our predictions for distributions of di-photons produced at the LHC. In Fig. 10 we plot the invariant mass and rapidity distribution of the photon pairs, and the

²When using the CTEQ4L PDF, we consistently use the LO running coupling constant α_s .

transverse momentum distribution of the individual photons. When plotting the transverse momentum distributions of the individual photons we include both photons per event. The total (upper solid) and the resummed $q\bar{q} + qg \rightarrow \gamma\gamma X$ (dashed), $q\bar{q} \rightarrow \gamma\gamma X$ (dotted), $gg \rightarrow \gamma\gamma X$ (dash-dotted), and the fragmentation (lower solid), as well as the leading order $q\bar{q} \rightarrow \gamma\gamma$ (middle solid) contributions are shown separately. The ratio of the resummed and the LO distributions is about 2.5 which is consistent with the result in Table I. The relative values of the contributions from each subprocesses reflect the summary given in Table III.

Fig. 11 shows various contributions to the transverse momentum of the photon pair. At low Q_T values ($Q_T \ll Q$), the $q\bar{q} \rightarrow \gamma\gamma X$ contribution is larger than the $qg \rightarrow \gamma\gamma X$ contribution, while at high Q_T values ($Q_T > Q$), the $qg \rightarrow \gamma\gamma X$ subprocess becomes more important. The gg contribution dominates the total rate in low Q_T region, and the kink in the gg curve at about 50 GeV indicates the need for the inclusion of the complete $\mathcal{O}(\alpha_s^3)$ $gg \rightarrow \gamma\gamma g$ contribution. (Recall that our prediction for the gg contribution at $\mathcal{O}(\alpha_s^3)$ only holds for small Q_T , where the effect of the initial-state soft-gluon radiation is relatively more important for a fixed Q .)

In Fig. 12 we give the integrated cross section as the function of the transverse momentum of the photon pair produced at the LHC. Similarly to the Z^0 pair production, there is a significant shape difference between the resummed and the NLO curves in the low to mid Q_T region. For $Q_T^{min} = 50$ GeV, the resummed rate is about 1.5 times of the NLO rate.

D. Di-photon production at the upgraded Tevatron

In Ref. [19], we have presented the predictions of the CSS resummation formalism for the di-photon production at the Tevatron with $\sqrt{S} = 1.8$ TeV, and compared with the data [21,22]. In this paper, we show the results for the upgraded Tevatron with $\sqrt{S} = 2.0$ TeV. We use the same kinematic cuts which were used in Ref. [19]:

$p_T^\gamma > 12$ GeV, for the transverse momentum of each photons,

$|y^\gamma| < 0.9$, for the rapidity of each photons.

An isolation cut of $\Delta R = 0.7$ is also applied. The total cross sections and the rates of the different subprocesses are given by Tables I and III. The ratio of the $q\bar{q} + qg \rightarrow \gamma\gamma X$ and $q\bar{q} \rightarrow \gamma\gamma$ rates is about 1.5, similar to that at the LHC. The leading order rate for the $gg \rightarrow \gamma\gamma$ subprocess is about 6.0 pb and 4.3 pb for using CTEQ4L and CTEQ4M PDF, respectively. The NLO rate for $gg \rightarrow \gamma\gamma g$ is estimated to be 8.3 pb, using the approximation described in Ref. [19], which is about the same magnitude as the leading order $q\bar{q} \rightarrow \gamma\gamma$ rate. From our estimate of the NLO gg rate, we expect that the complete $\mathcal{O}(\alpha_s^3)$ contribution will be important for photon pair production at the Tevatron.

Figs. 13–15 show our results for photon pairs produced at the upgraded Tevatron. The resummed predictions for the invariant mass and rapidity distributions of the photon pairs, and the transverse momentum distribution of the individual photons are shown in Fig. 13. In Fig. 14 we also plot the contributions to the transverse momentum of the photon pair from the $q\bar{q} + qg \rightarrow \gamma\gamma X$ (dashed), $q\bar{q} \rightarrow \gamma\gamma X$ (dotted), $gg \rightarrow \gamma\gamma g$ (dash-dotted), and the fragmentation (lower solid) subprocesses, separately. The leading order $q\bar{q} \rightarrow \gamma\gamma$ cross section (middle solid) is also plotted. In the low Q_T region, the gg and the $q\bar{q}$ rates are about the same, and the qg rate becomes more important in the large Q_T region. Furthermore, after imposing the above kinematic cuts, the fragmentation contribution is found to be unimportant.

Fig. 15 shows the integrated Q_T distribution. The qualitative features of these distributions are the same as those predicted for the LHC. For $Q_T^{min} = 10$ GeV, the resummed cross section is about twice of the NLO cross section.

IV. CONCLUSIONS

In this work we studied the effects of the initial-state multiple soft-gluon emission on the total rates and various distributions of the most important background processes ($pp, p\bar{p} \rightarrow \gamma\gamma X, Z^0 Z^0 X$) to the detection of the Higgs boson at the LHC. We applied the extended CSS formalism to resum the large logarithms induced by the soft-gluon radiation. We

found that for the $q\bar{q}$ and qg initiated processes, the total cross sections and the invariant mass distributions of the photon and Z^0 boson pairs are in agreement with the fixed order calculations. From our estimate of the NLO rate of the gg initiated process, we expect that the complete $\mathcal{O}(\alpha_s^3)$ contribution will be important for photon pair production at the Tevatron. We showed that the resummed and the NLO transverse momentum distributions of the Z^0 and photon pairs are substantially different for $Q_T \lesssim Q/2$. In terms of the integrated cross section above a given Q_T^{\min} , this difference can be as large as 50% in the low to mid-range of Q_T^{\min} . Using the resummation calculation, we are able to give a reliable prediction of the Q_T and any other distribution in the full kinematical region at the LHC and the Tevatron, even in the presence of kinematic cuts. Since the bulk of the signal is in the low transverse momentum region, we conclude that the difference between the NLO and resummed predictions of the background rates will be essential when extracting the signal of the Higgs boson at hadron colliders.

ACKNOWLEDGMENTS

We thank the CTEQ collaboration, E. Berger, S. Mrenna, W. Repko and C. Schmidt for many invaluable discussions, J. Huston and M. Abolins for help with the ATLAS parameters and for useful conversations. C.B. also thanks the Theory Division of FermiLab for the invitation and hospitality. This work was supported in part by the NSF under grant PHY-9802564.

REFERENCES

- [1] ALEPH Collaboration (R. Barate et al.), preprint: ALEPH 98-029, CONF 98-017; L3 Higgs Working Group (M. Biasini et. al), preprint: L3 note 2237; OPAL Collaboration (G. Abbiendi et al.), e-print: hep-ex/9811025.
- [2] J. Erler, P. Langacker, preprint: UPR-791-T, e-print: hep-ph/9801422; J. Erler, P. Langacker, preprint: UPR-816-T, e-print: hep-ph/9809352.
- [3] S. Parke, preprint: FERMILAB-CONF-97-335-T, e-print: hep-ph/9710351.
- [4] S. Heinemeyer, W. Hollik, G. Weiglein, preprint: KA-TP-2-1998, e-print: hep-ph/9803277; M. Brhlik, G.L. Kane, preprint: UM-TH-98-07, eprint: hep-ph/9803391.
- [5] D. Amidei, R. Brock, editors, *Future Electroweak Physics at the Fermilab Tevatron*, report FERMILAB-PUB-96/082 (1996); S. Kim, S. Kuhlmann, W.-M. Yao, in *Proceedings of the 1996 DPF/DBP Summer Study on New Directions for High Energy Physics* (1996); S. Mrenna, in *Perspectives on Higgs Physics II*, ed. G.L. Kane, (World Scientific, Singapore, 1997), p. 131; CDF Collaboration (F. Abe et al.), preprint: FERMILAB-PUB-98-252-E.
- [6] T. Han, R.-J. Zhang, preprint: MADPH-98-1067, e-print: hep-ph/9807424.
- [7] M. Drees, M. Guchait, P. Roy, Phys. Rev. Lett. **80**, 2047 (1998); Erratum-ibid. **81**, 2394 (1998); J.L. Diaz-Cruz, H.-J. He, T. Tait and C.-P. Yuan, Phys. Rev. Lett. **80**, 4641 (1998); H. Baer, B.W. Harris, X. Tata, preprint: FSU-HEP-980626, e-print: hep-ph/9807262; C. Balázs, J.L. Diaz-Cruz, H.J. He, T. Tait, C.-P. Yuan, preprint: MSUHEP-80515, e-print: hep-ph/9807349, submitted to *Phys. Rev. D*;

M. Carena, S. Mrenna, C.E.M. Wagner, preprint: ANL-HEP-PR-98-54, e-print: hep-ph/9808312.

[8] ATLAS collaboration, preprint: CERN/LHC/94-43 LHCC/P2 (1994);
 CMS collaboration, preprint: CERN/LHC/94-43 LHCC/P1 (1994).

[9] A. Djouadi, M. Spira and P. M. Zerwas, *Phys. Lett.* **B264** 440 (1991);
 S. Dawson, *Nucl. Phys.* **B359** 283 (1991);
 D. Graudenz, M. Spira and P. M. Zerwas, *Phys. Rev. Lett.* **70** , 1372 (1993);
 M. Spira, A. Djouadi, D. Graudenz and P. M. Zerwas, *Phys. Lett.* **B318** 347 (1993);
 R. P. Kauffman and W. Schaffer, *Phys. Rev.* **D49** 551 (1994);
 S. Dawson and R.P. Kauffman, *Phys. Rev.* **D49**, 2298 (1994);
 M. Spira, A. Djouadi, D. Graudenz and P.M. Zerwas, *Nucl. Phys.* **B453**, 17 (1995).

[10] J.F. Owens, J. Ohnemus, *Phys. Rev.* **D46**, 2018 (1992).

[11] B. Mele, P. Nason, G. Ridolfi, *Nucl. Phys.* **B357**, 409 (1991).

[12] E.L. Berger, E. Braaten, R.D. Field, *Nucl. Phys.* **B239**, 52 (1984);
 P. Aurenche, A. Douiri, R. Baier, M. Fontannaz, D. Schiff, *Z. Phys C* **29**, 459 (1985);
 B. Bailey, J.F. Owens and J. Ohnemus, *Phys. Rev.* **D46**, 2018 (1992).

[13] M. Krämer, E. Laenen, M. Spira, *Nucl. Phys.* **B511**, 523 (1998).

[14] S. Abdullin, M. Dubinin, V. Ilyin, D. Kovalenko, V. Savrin, N. Stepanov,
Phys. Lett. **B431**, 410 (1998).

[15] C. Balázs, C.-P. Yuan, *Higgs Boson Production at Hadron Colliders with Soft Gluon Effects: II. The Signal*, in preparation.

[16] J. Collins, D. Soper, *Nucl. Phys.* **B193**, 381 (1981);
Nucl. Phys. **B213**, 545(E) (1983); *Nucl. Phys.* **B197**, 446 (1982).

[17] J. C. Collins, D. Soper, G. Sterman, *Phys. Lett.* **B109**, 388 (1982);
Nucl. Phys. **B223**, 381 (1983); *Phys. Lett.* **B126**, 275 (1983).

[18] J. C. Collins, D. Soper, G. Sterman, *Nucl. Phys.* **B250**, 199 (1985).

[19] C. Balázs, E. Berger, S. Mrenna, C.-P. Yuan, *Phys. Rev.* **D57**, 6934 (1998).

[20] T. Han, R. Meng, J. Ohnemus, *Nucl. Phys.* **B384**, 59 (1992).

[21] L. Nodulman, in *ICHEP '96, Proceedings of the 28th International Conference on High Energy Physics*, Warsaw, 1996, ed. by Z. Ajduk and A.K. Wroblewski (World Scientific, Singapore, 1997), p. 1064.

[22] D0 Collaboration (P. Hanlet for the collaboration), *Nucl. Phys. Proc. Suppl.* **64**, 78 (1998).

[23] T. Barklow et al., in *Proceedings of the 1996 DPF/DBP Summer Study on New Directions for High Energy Physics*, e-print: hep-ph/9611454;
I. Kuss, E. Nuss, *Eur. Phys. J.* **C4**, 641 (1998);
H.T. Diehl, e-print: hep-ex/9810006.

[24] C. Balázs and C.-P. Yuan, *Phys. Rev.* **D56**, 5558 (1997).

[25] J. Collins, D. Soper, *Phys. Rev.* **D16** (1977) 2219.

[26] G.A. Ladinsky and C.-P. Yuan, *Phys. Rev.* **D50**, 4239 (1994).

[27] E.W.N. Glover, J.J. van der Bij, *Nucl. Phys.* **B313**, 237 (1989);
J.J. van der Bij, E.W.N. Glover, *Nucl. Phys.* **B321**, 561 (1989).

[28] V.N. Gribov, L.N. Lipatov, *Yad. Phys.* **15**, 781 (*Sov. J. Nucl. Phys.* **15**, 438) (1972);
L.N. Lipatov, *Yad. Phys.* **20**, 181 (*Sov. J. Nucl. Phys.* **20**, 94) (1975);
Yu.L. Dokshitzer, *Sov. Phys. JETP* **46**, 641 (1977);
G. Altarelli, G. Parisi, *Nucl. Phys.* **B126**, 298 (1977);

G. Altarelli, *Phys. Rep.* **81**, 1 (1982).

[29] B. Bailey, J.F. Owens and J. Ohnemus, *Phys. Rev.* **D46**, 2018 (1992).

[30] H.L. Lai et al., *Phys. Rev.* **D55**, 1280 (1997).

[31] C.-P. Yuan, Talk given at 33rd Rencontres de Moriond: *QCD and High Energy Hadronic Interactions, Les Arcs, France, 21-28 Mar 1998*. e-print: hep-ph/9807316.

[32] Review of Particle Physics, *The European Physical Journal* **C3**, 1 (1998).

[33] V. Barger, J.L. Lopez, W. Putikka, *Int. J. Mod. Phys.* **A3**, 2181 (1988).

Di-boson produced	Collision type	\sqrt{S} (TeV)	Fixed Order $\mathcal{O}(\alpha_s^0)$	Resummed
			CTEQ4L	$\oplus \mathcal{O}(\alpha_s)$
$Z^0 Z^0$	pp	14	9.14	14.8
$Z^0 Z^0$	$p\bar{p}$	2	0.91	1.64
$\gamma\gamma$	pp	14	22.1	60.8
$\gamma\gamma$	$p\bar{p}$	2	8.48	22.8
$\gamma\gamma$	$p\bar{p}$	1.8	6.30	7.15
				17.0

TABLE I. Total cross sections of di-photon and Z^0 boson pair production at the LHC and the upgraded Tevatron, in units of pb. The kinematic cuts are described in the text. The “ \oplus ” sign refers to the matching prescription discussed in the text.

\sqrt{S} (TeV)	Collision type	$q\bar{q} \rightarrow Z^0 Z^0 X$	$qg \rightarrow Z^0 Z^0 X$
14	pp	10.9	3.91
2	$p\bar{p}$	1.62	0.02

TABLE II. Resummed cross sections of the subprocesses for Z^0 boson pair production at the LHC and the upgraded Tevatron, in units of pb. The kinematic cuts are described in the text.

\sqrt{S} (TeV)	Collision type	$q\bar{q} \rightarrow \gamma\gamma X$	$qg \rightarrow \gamma\gamma X$	$gg \rightarrow \gamma\gamma$	$gg \rightarrow \gamma\gamma g$	$qg \rightarrow \gamma qX \rightarrow \gamma\gamma X'$	Fragmentation
		$\mathcal{O}(\alpha_s^2)$	4L	$\mathcal{O}(\alpha_s^2)$	4M		
14	pp	20.5	16.6	22.3	14.4	23.9	6.76
2	$p\bar{p}$	9.68	4.81	6.02	4.34	8.26	2.15

TABLE III. Cross sections of the subprocesses for di-photon production at the LHC and the upgraded Tevatron, in units of pb. The resummed $qg \rightarrow \gamma\gamma X$ rate includes the fragmentation contribution. The $\mathcal{O}(\alpha_s^2)$ $gg \rightarrow \gamma\gamma$ rates were calculated using both the CTEQ4L and CTEQ4M PDF's. The kinematic cuts are described in the text.

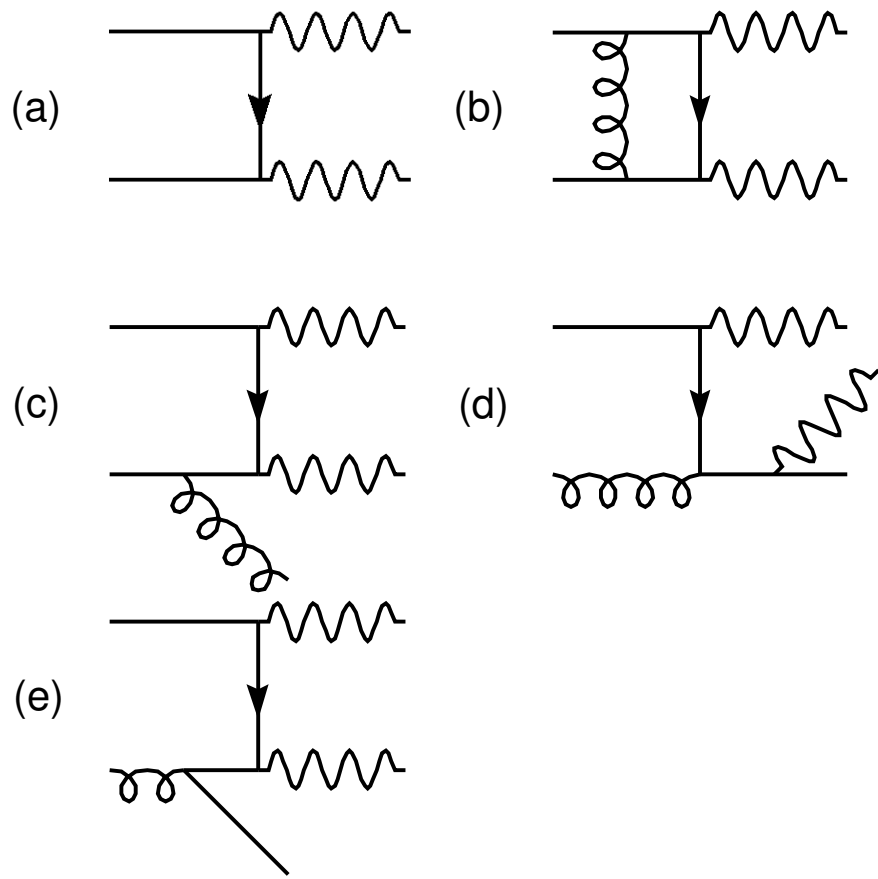


FIG. 1. A representative set of Feynman diagrams included in the NLO calculation of Z^0 pair production.

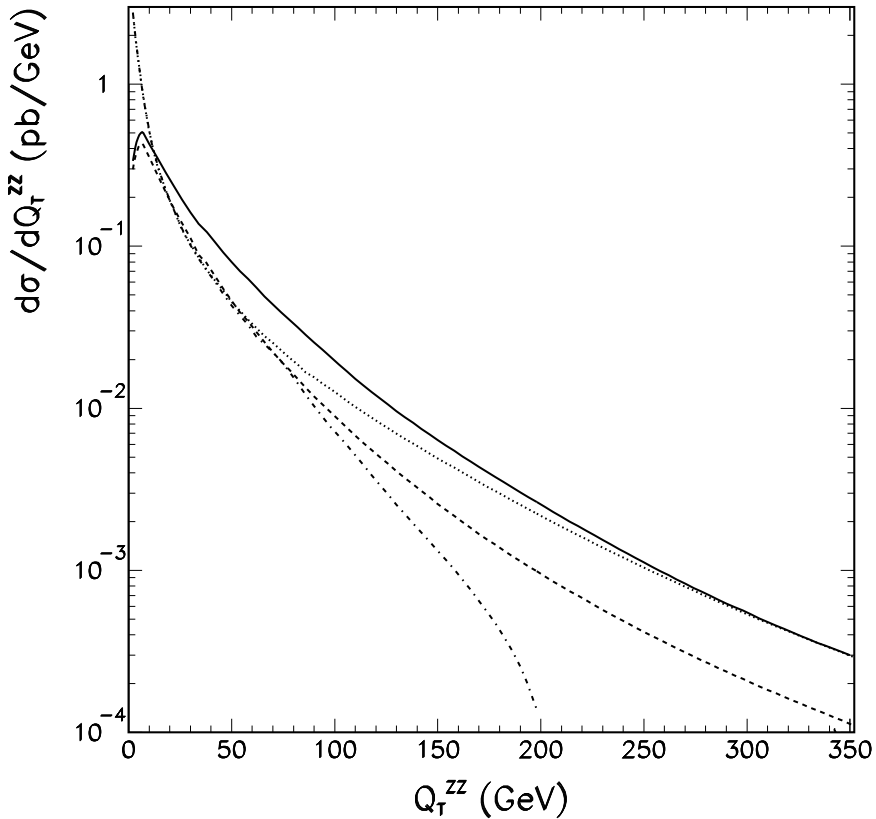


FIG. 2. Transverse momentum distribution of Z^0 pairs from $q\bar{q} + qg$ partonic initial states at the LHC. The $\mathcal{O}(\alpha_s)$ (dotted) and the asymptotic (dash-dotted) pieces coincide and diverge as $Q_T \rightarrow 0$. The resummed (solid) curve matches the $\mathcal{O}(\alpha_s)$ curve at about $Q_T = 320$ GeV. The resummed $q\bar{q}$ contribution (excluding the qg contribution) is shown as dashed line.

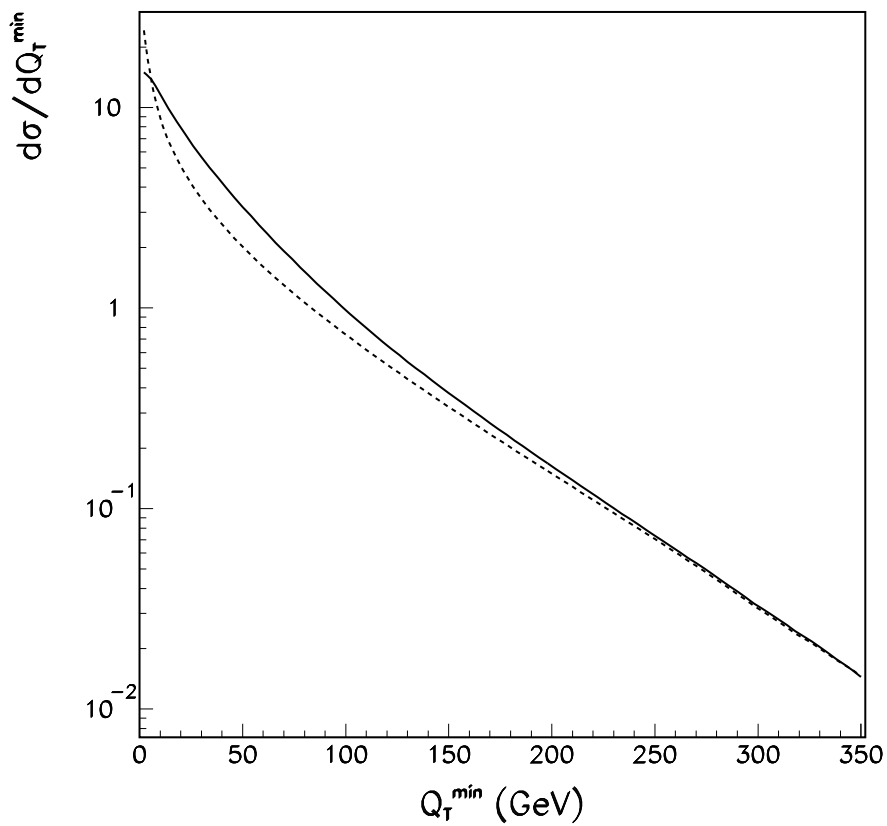


FIG. 3. The integrated cross section for Z^0 boson pair production at the LHC. The resummed and the $\mathcal{O}(\alpha_s)$ distributions are shown in solid and dashed lines, respectively.

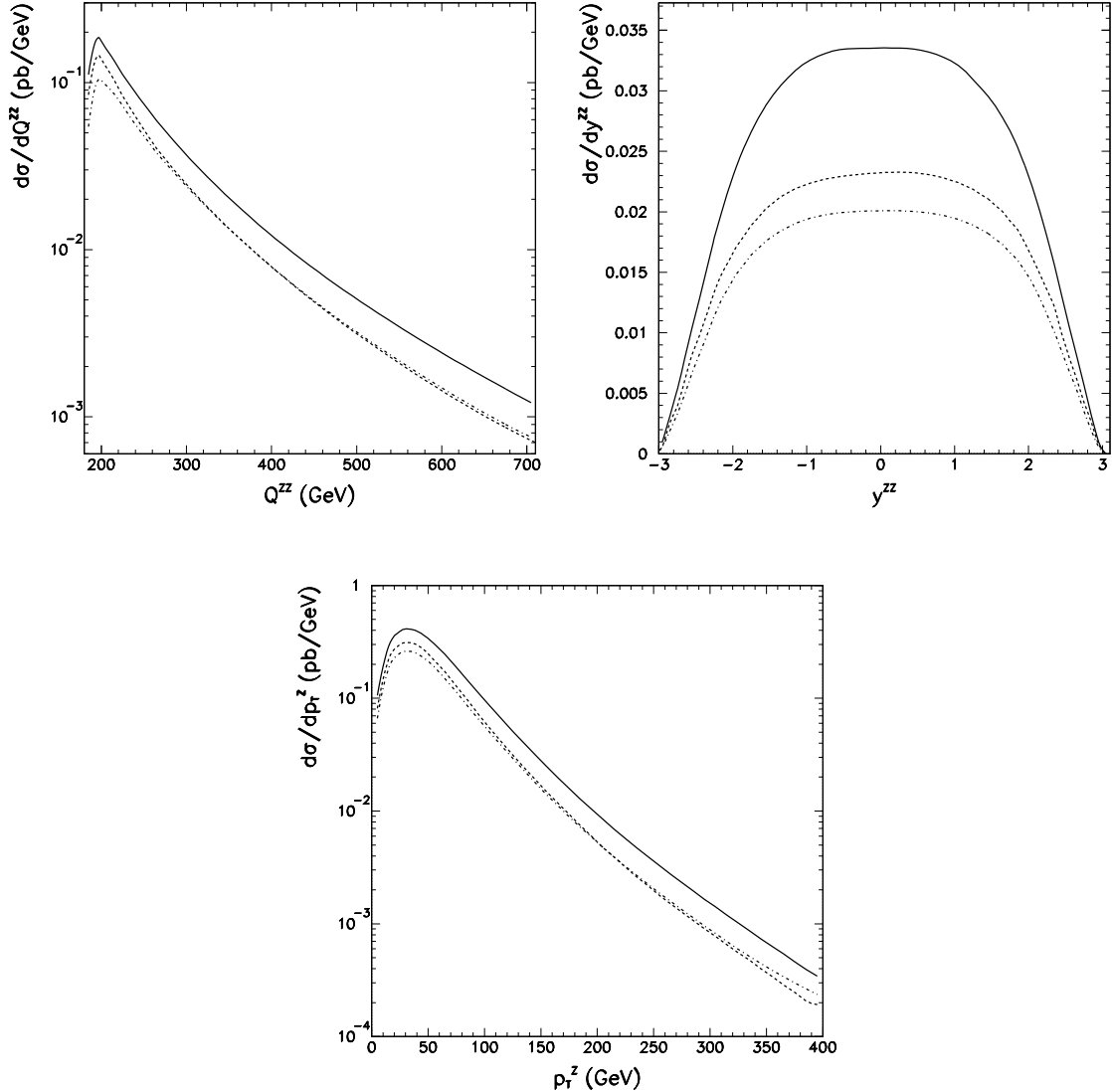


FIG. 4. Invariant mass and rapidity distributions of Z^0 boson pairs, and transverse momentum distributions of the individual Z^0 bosons at the LHC. The resummed contribution of the $q\bar{q} + qg \rightarrow Z^0 Z^0 X$ subprocess is shown by the solid curve, and of the $q\bar{q} \rightarrow Z^0 Z^0 X$ subprocess by the dashed curve. The leading order distribution of $q\bar{q} \rightarrow Z^0 Z^0$ is shown by the dash-dotted curve.

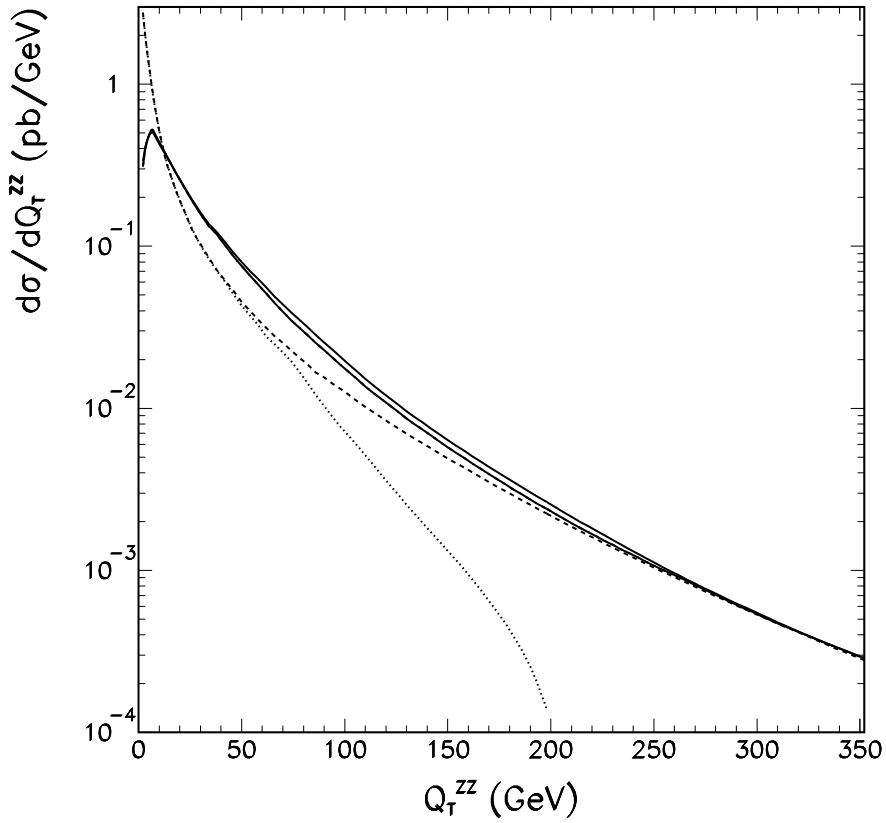


FIG. 5. Resummed and NLO transverse momentum distributions of Z^0 boson pairs at the LHC. The two resummed curves are calculated for $C_1 = b_0$ and $C_2 = 1$ (upper solid), and for $C_1 = b_0/2$ and $C_2 = 1/2$ (lower solid), respectively. The NLO curves are the same as in Fig. 2.

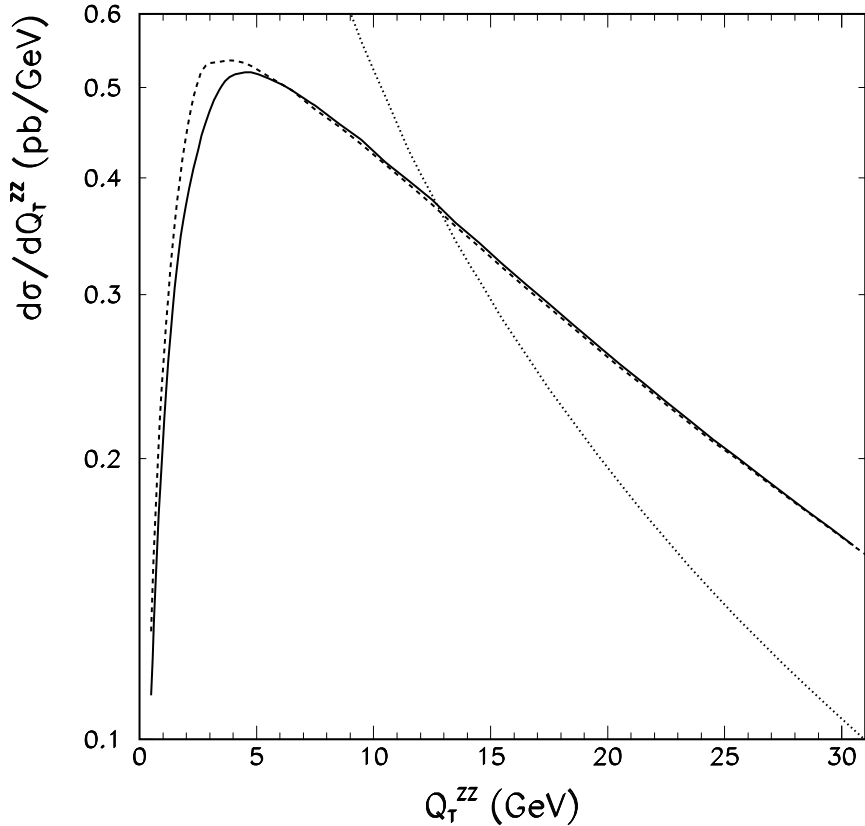


FIG. 6. Resummed and NLO transverse momentum distributions of Z^0 boson pairs at the LHC. The two resummed curves are calculated for $g_1 = 0.11 \text{ GeV}^2$, $g_2 = 0.58 \text{ GeV}^2$, and $g_3 = -1.5 \text{ GeV}^{-1}$ (solid), and for $g_1 = 0.15 \text{ GeV}^2$, $g_2 = 0.48 \text{ GeV}^2$, and $g_3 = -0.58 \text{ GeV}^{-1}$ (dashed), respectively. In both cases $Q_0 = 1.6 \text{ GeV}$ was used. The NLO (dotted) curve is the same as in Fig. 2.

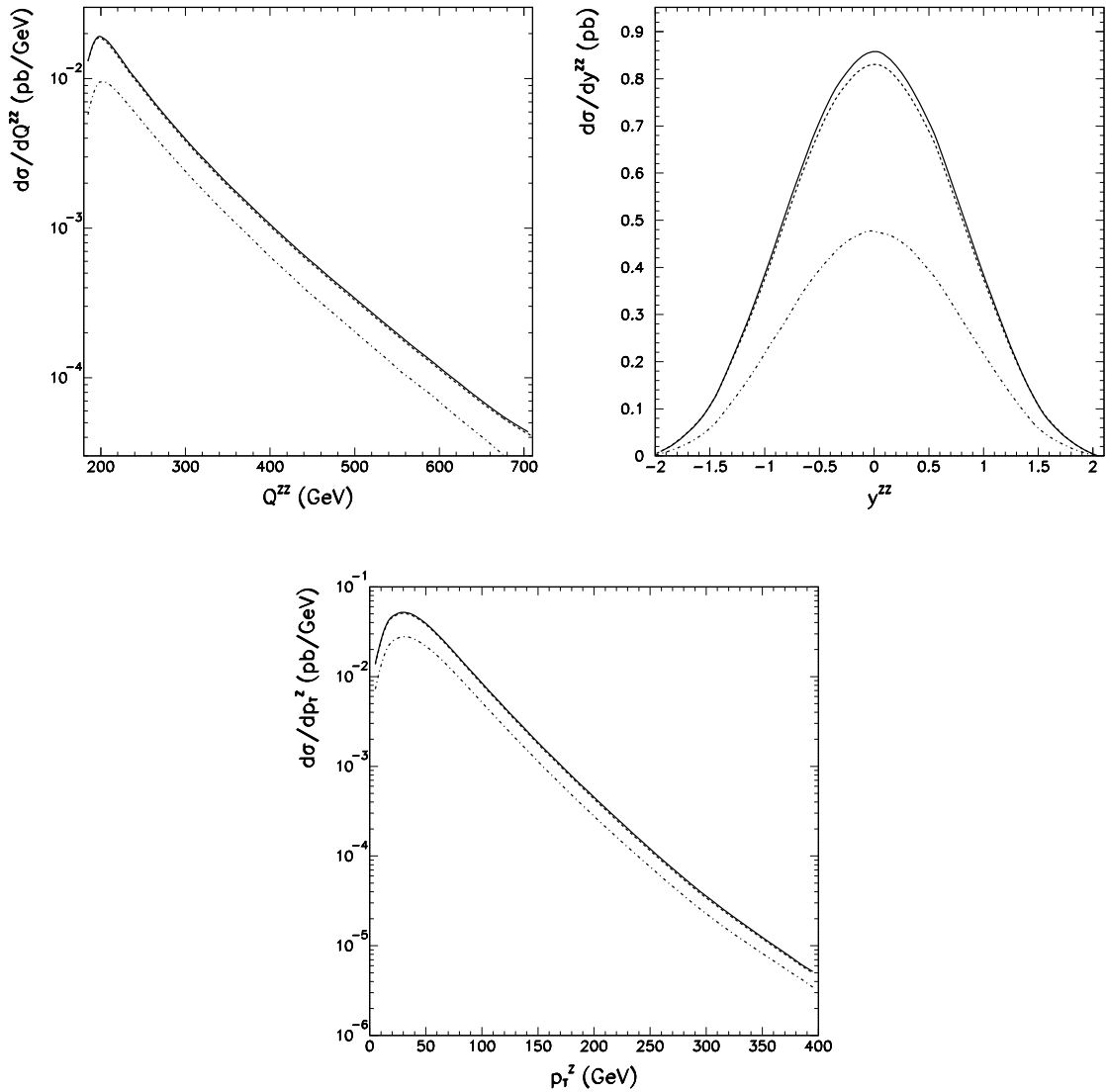


FIG. 7. Same as Fig. 4 except for the upgraded Tevatron.

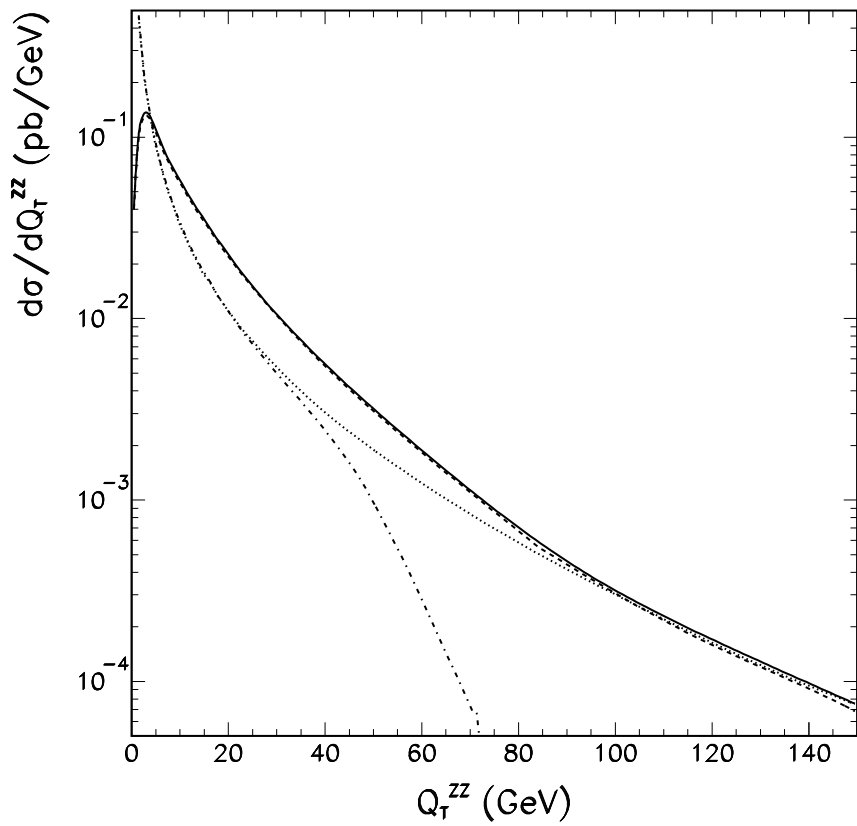


FIG. 8. Same as Fig. 2 except for the upgraded Tevatron.

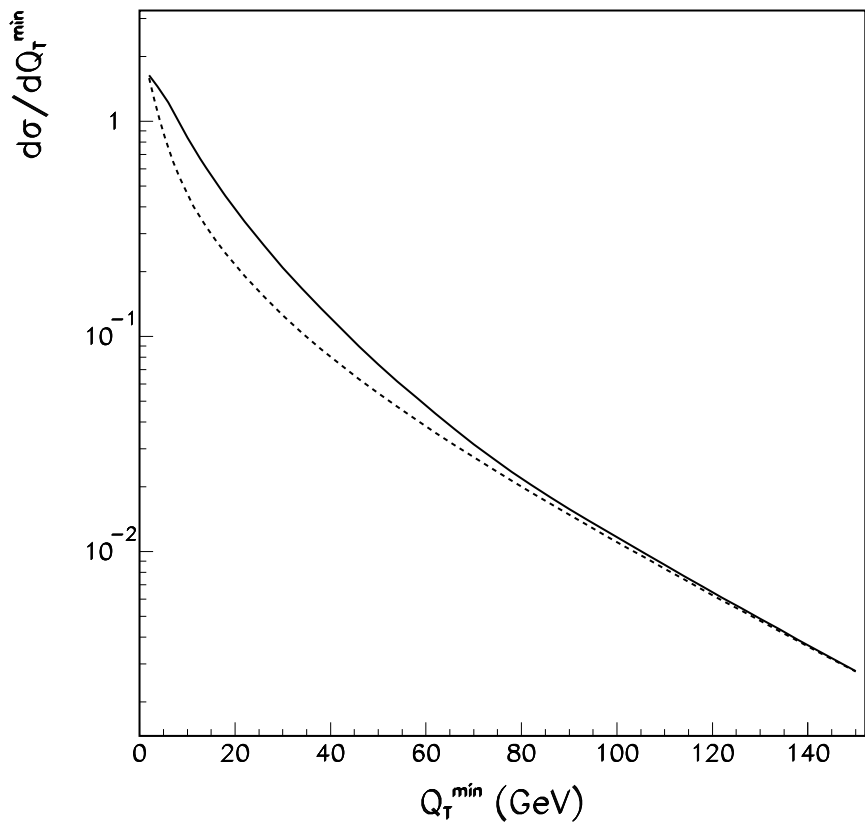


FIG. 9. Same as Fig. 3 except for the upgraded Tevatron.

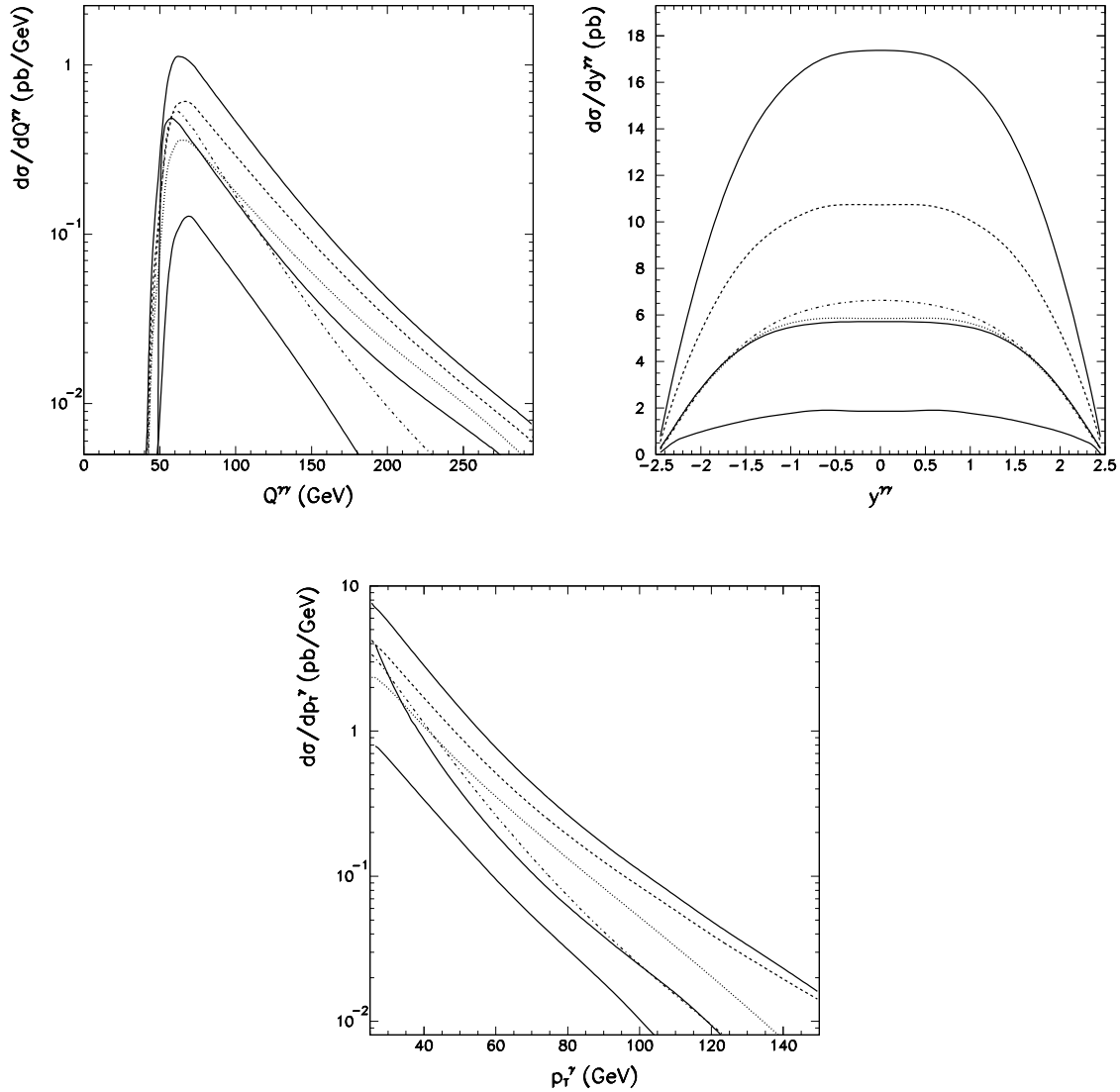


FIG. 10. Invariant mass and rapidity distributions of photon pairs, and transverse momentum distributions of the individual photons at the LHC. The total resummed contribution (upper solid), and the resummed $q\bar{q} + qg \rightarrow \gamma\gamma X$ (dashed), $q\bar{q} \rightarrow \gamma\gamma X$ (dotted), $gg \rightarrow \gamma\gamma g$ (dash-dotted), as well as the fragmentation (lower solid) contributions are shown separately. The $q\bar{q} \rightarrow \gamma\gamma \mathcal{O}(\alpha_s^0)$ distribution is shown in the middle solid curve.

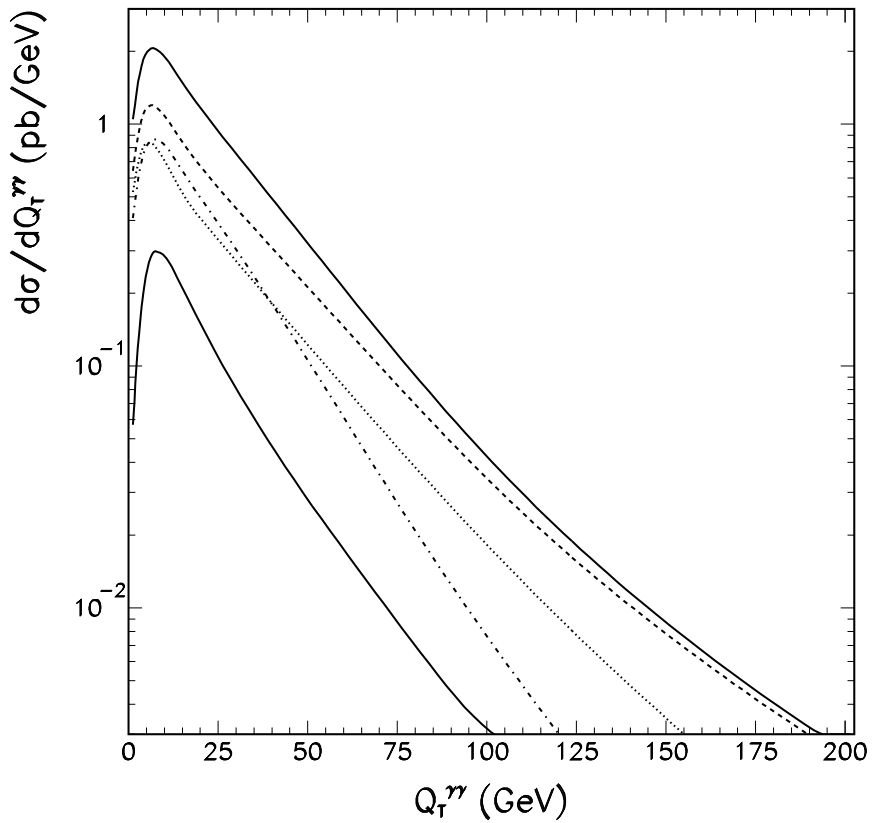


FIG. 11. Transverse momentum distribution of photon pairs at the LHC. The total resummed contribution (upper solid), the resummed $q\bar{q} + qg \rightarrow \gamma\gamma X$ (dashed), $q\bar{q} \rightarrow \gamma\gamma X$ (dotted), $gg \rightarrow \gamma\gamma X$ (dash-dotted), as well as the fragmentation (lower solid) contributions are shown separately.

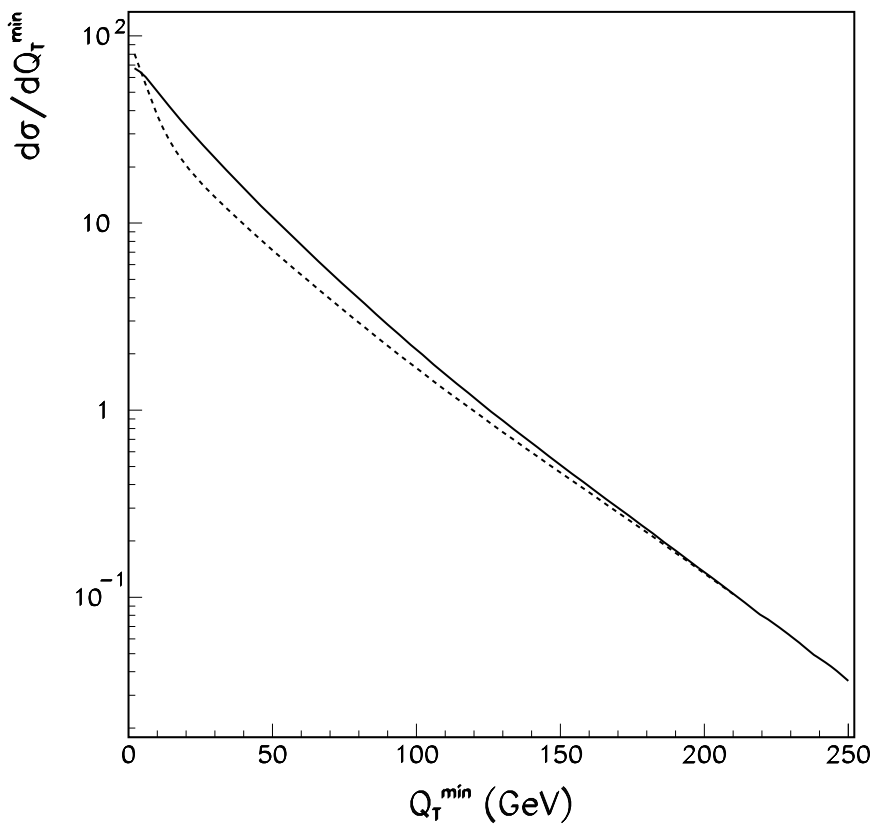


FIG. 12. The integrated cross section for photon pair production at the LHC. The resummed and the $\mathcal{O}(\alpha_s)$ distributions are shown in solid and dashed lines, respectively.

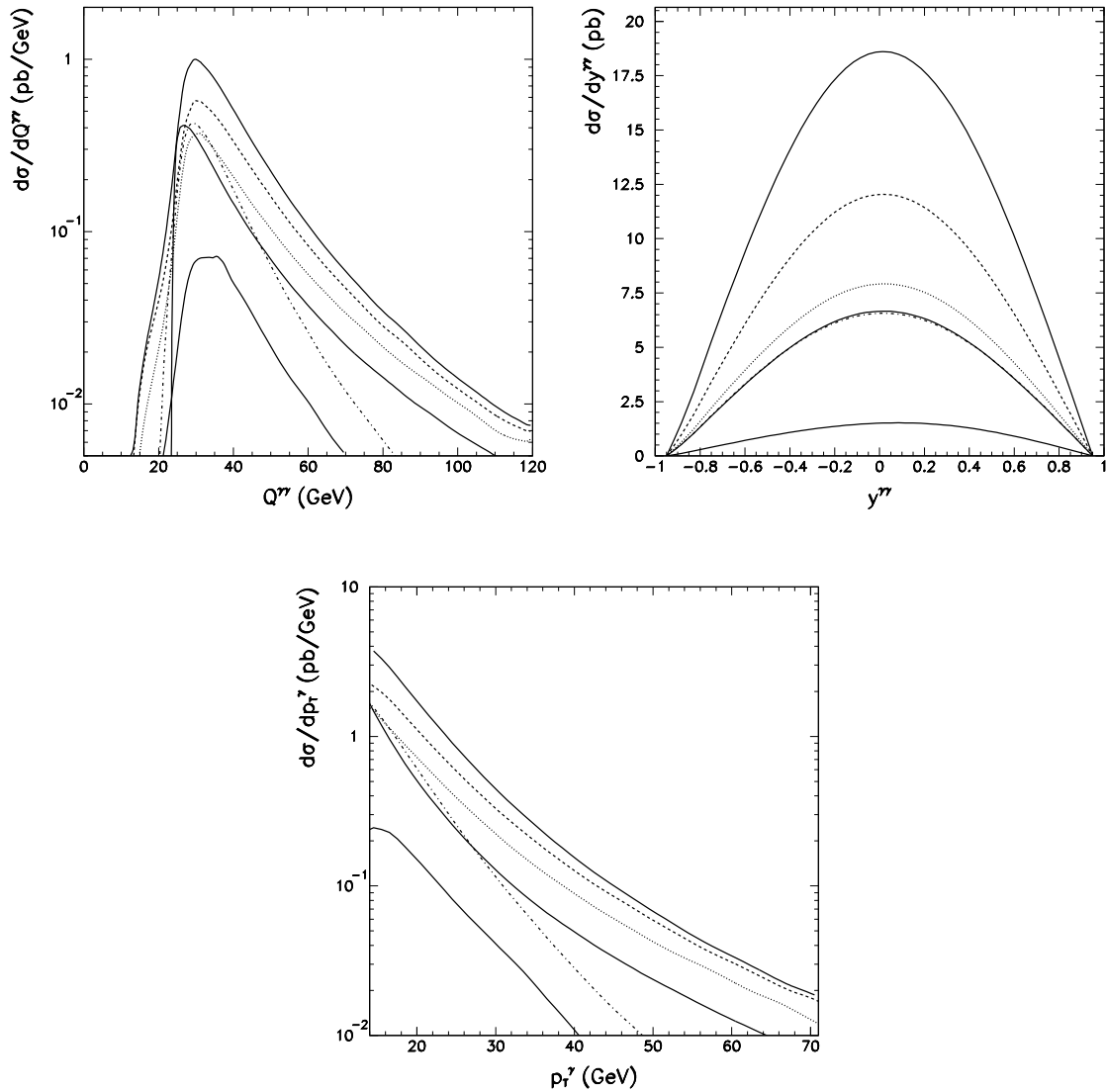


FIG. 13. Same as Fig. 10 but for the upgraded Tevatron.

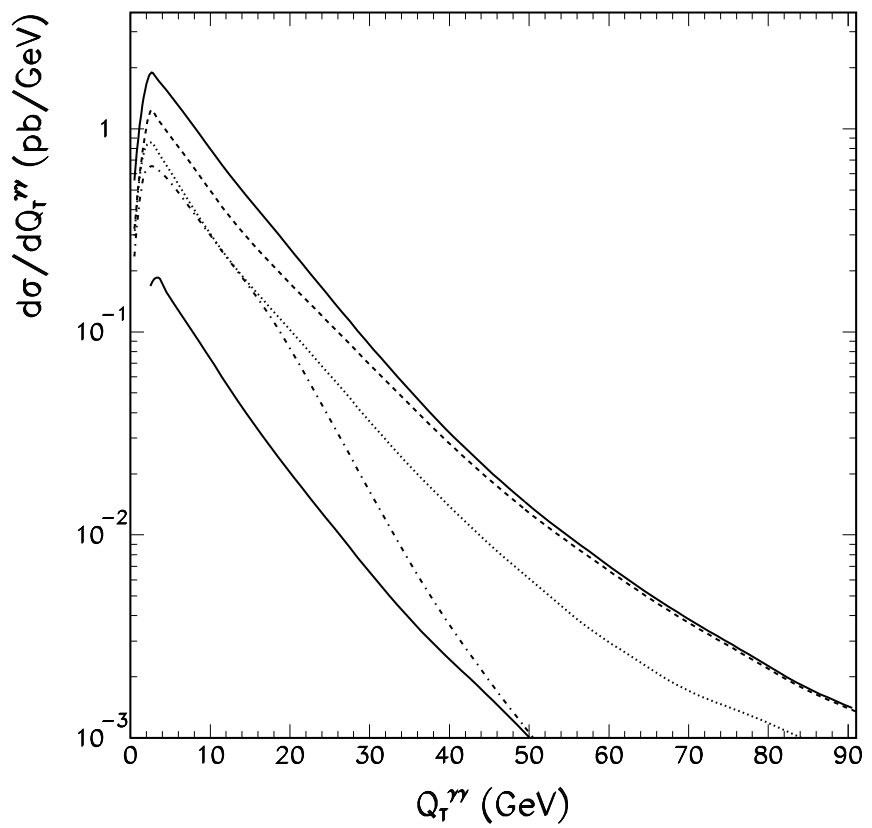


FIG. 14. Same as Fig. 11 but for the upgraded Tevatron.

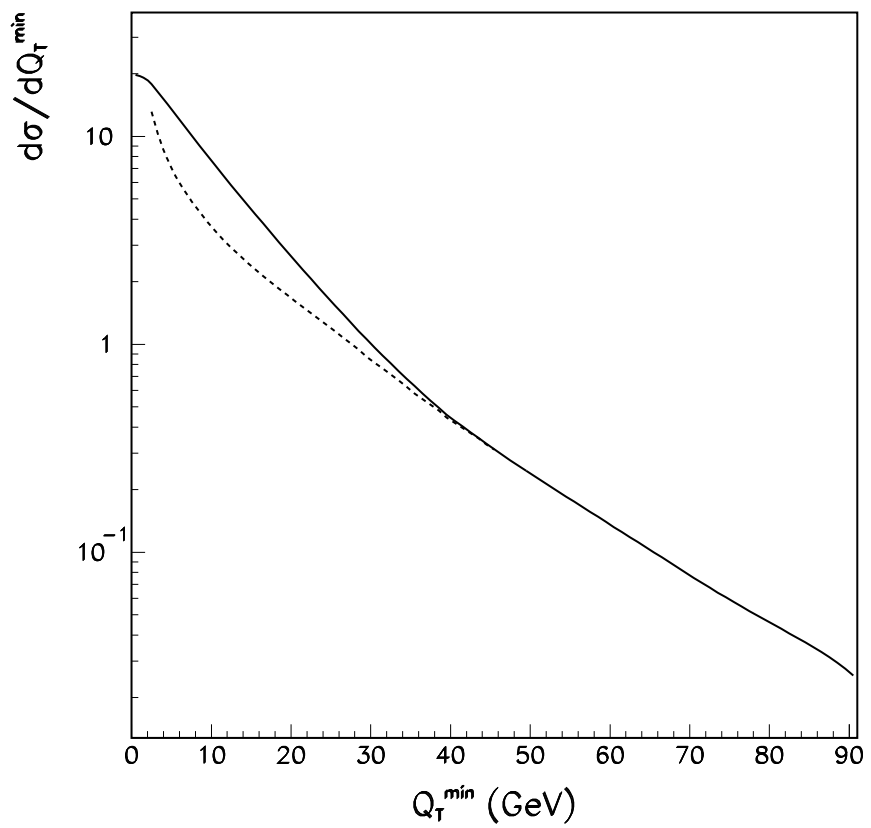


FIG. 15. Same as Fig. 12 but for the upgraded Tevatron.